J|A|C|S ARTICLES

Published on Web 06/16/2009

trans-2 Addition Pattern to Power Charge Transfer in Dendronized Metalloporphyrin C_{60} Conjugates

Fabian Spänig,[†] Michaela Ruppert,[‡] Jörg Dannhäuser,[‡] Andreas Hirsch,*[,‡] and Dirk M. Guldi*[,†]

Department of Chemistry and Pharmacy and Interdisciplinary Center of Molecular Materials (ICMM), Friedrich-Alexander Universität Erlangen Nürnberg, Egerlandstrasse 3, 91058 Erlangen, Germany, and Department of Chemistry and Pharmacy and Interdisciplinary Center of Molecular Materials (ICMM), Friedrich-Alexander Universität Erlangen Nürnberg, Henkestrasse 42, 91054 Erlangen, Germany

Received April 14, 2009; E-mail: guldi@chemie.uni-erlangen.de; andreas.hirsch@chemie.uni-erlangen.de

Abstract: Coordinating different transition metals—manganese(III), iron(III), nickel(II), and copper(II)—by a dendronized porphyrin afforded a new family of redox-active metalloporphyrins to which C_{60} was attached as a ground-state electron acceptor. Such a strategy introduced an additional center of redoxactivity, that is, a change of the oxidation state of the metal. Cyclic voltammetry and absorption/fluorescence measurements provided support for mutual interactions between the redox-active constituents in the ground state. In particular, slightly anodic shifted reduction potentials/cathodic shifted oxidation potentials and the occurrence of new charge transfer features in the 700−900 nm range prompt to sizable electronic coupling in the range of 300 cm^{-1}. Photophysical means—steady-state/time-resolved fluorescence and transient absorption measurements—shed light on the excited-state interactions. To this end, we have added pulse radiolytic investigations to characterize the radical cation (i.e., metalloporphyrins) and radical anion (i.e., fullerene) characteristics. $\pi-\pi$ stacking of the excited state electron donor and the electron acceptor is key to overcome the intrinsically fast deactivation of the excited states in these metalloporphyrins and to power an exothermic charge transfer. The lifetimes of the rapidly and efficiently generated radical ion pair states, which range from 15 to >3000 ps, revealed several important trends. First, they were found to depend on the solvent polarity. Second, the nature of the transition metal plays a similarly decisive role. It is important that the product of charge recombination, namely tripmultiplet excited states versus ground state, had a great impact. Finally, a correlation between the charge transfer rate (i.e., charge separation and charge recombination) and the free energy change for the underlying reaction reveals a parabolic dependence with parameters of the reorganization energy (0.84 eV) and electronic coupling (70 cm^{-1}) closely resembling that seen for the zinc(II) and free base analogues.

Introduction

One of the ultimate goals of molecular electronics is the rational design of electron donor−acceptor conjugates/hybrids capable of light-induced charge-separation over long distances on the molecular scale. In this context, ultrafast charge-transfer systems will likely figure prominently in proposed photodriven molecular-scale rectifiers and emerging technologies that focus on light-modulated data storage and retrieval.[1−4]

There has been considerable interest in electron donor−acceptor systems, in which C_{60} serve as electron and energy acceptors upon photoexcitation.[5−8] While a large variety of such systems have been synthesized and subjected to photophysical investigation, the greatest attention has been paid to systems in which porphyrins are linked to C_{60} by a variety of flexible, rigid, and semirigid linkers.[9,10]

C_{60} and porphyrins are molecular architectures ideally suited for devising integrated, multicomponent model systems to transmit and process solar energy. The implementation of C_{60} as a three-dimensional electron acceptor[11] holds great expectations on account

[†] Egerlandstrasse 3.
[‡] Henkestrasse 42.

(1) *An Introduction to Molecular Electronics*; Petty M. C., Bryce M. R., Bloor, D., Eds.; Oxford University Press: New York, 1995.
(2) *Molecular Electronics*; Jortner J., Ratner M., Eds.; Blackwell: Oxford, 1997.
(3) Fox, M. A. *Acc. Chem. Res.* **1999**, *32*, 201.
(4) Carroll, R. L.; Gorman Christopher, B. *Angew. Chem., Int. Ed.* **2002**, *41*, 4378.
(5) Guldi, D. M. *Chem. Commun.* **2000**, 321.
(6) Guldi, D. M. The Small Reorganization Energy of Fullerenes. In *Fullerenes: From Synthesis to Optoelectronic Properties*; Guldi, D. M., Martin, N., Eds.; Kluwer Academic Publishers: Norwell, MA, 2002; p 237.
(7) Guldi, D. M.; Kamat, P. V. Photophysical Properties of Pristine Fullerenes and Fullerene-Containing Donor-Bridge-Acceptor Systems. In *Chemistry, Physics and Technology*; Kadish, K. M., Ruoff, R. S., Eds.; John Wiley and Sons: New York, 2000; p 225.
(8) Martin, N.; Sanchez, L.; Illescas, B.; Perez, I. *Chem. Rev.* **1998**, *98*, 2527.
(9) Schuster, D. I. *Carbon* **2000**, *38*, 1607.
(10) Bracher, P. J.; Schuster, D. I. Electron Transfer in Functionalized Fullerenes. In *Fullerenes: From Synthesis to Optoelectronic Properties*; Guldi, D. M., Martin, N., Eds.; Kluwer Academic Publishers: Norwell, MA, 2002; p 163.
(11) *Fullerenes and Related Structures*; Hirsch, A., Ed; Springer: Berlin, 1999; Vol. 199.

 10.1021/ja9029686 CCC: $40.75

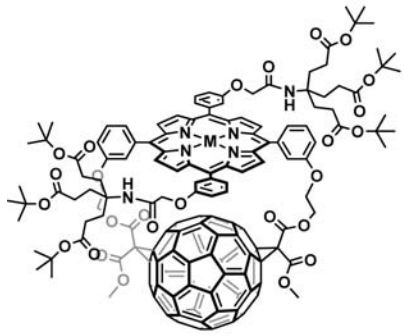

M-1

M = 2H, Zn, Cu, Co, Ni, Mn(Cl), Fe(Cl)

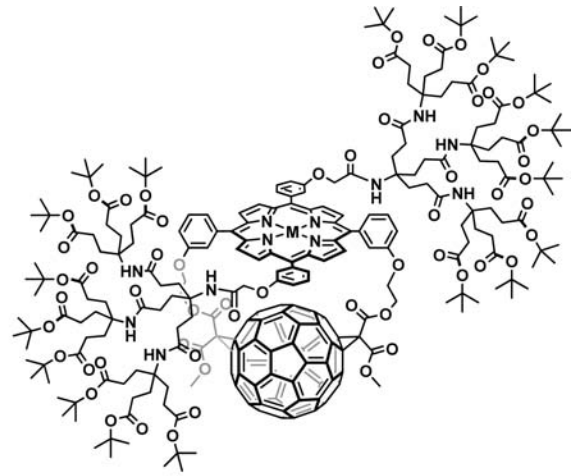

M-2

M = 2H, Zn, Cu, Co, Ni, Mn(Cl); Fe(Cl)

of its small reorganization energy in electron transfer reactions,[12−15] which has exerted a noteworthy impact on the development of C_{60}-based materials for applications involving light-induced charge-separation.[5,6,8,16−27] Due to van der Waals attraction between C_{60} and porphyrins, electron donor−acceptor conjugates/hybrids tend to adopt conformations, where these moieties achieve close spatial proximity. To this end, several groups have successfully constructed doubly linked conjugates, in which C_{60} and porphyrins are brought into close proximity (i.e., $\pi-\pi$ stacking).[28−38] In fact, the center-to-center distance is in the order of 6.5−7.0 Å. Charge transfer, upon excitation, in such systems is extremely fast, occurring in the picosecond time domain, usually to the exclusion of intramolecular energy transfer. Notable, in systems with larger center-to-center distance, both charge transfer and energy transfer occur. Then, the polarity of the solvent emerged as a crucial parameter in regulating the competition between the two processes.[39,40]

We have become interested in how redox-active metal centers, such as transition metals, affect the nature and dynamics of an intramolecular electronic dialogue. For instance, the choice of paramagnetic metals creates a particularly interesting scenario, since augmented electronic coupling is expected to enhance charge transfer processes. However, such aspects have hardly ever been addressed.[30,41−43] Ultrafast excited state deactivation of the metalloporphyrins, due to efficient spin-orbit coupling and mixing with d-states, is largely responsible for this rareness. The success in probing, for example, metalloporphyrins–with manganese, iron, nickel, cobalt, and copper–as photoexcited state electron donors depends on overcoming the fast excited state deactivations. An obvious strategy would involve an intramolecular charge separation event that is substantially fast. One requisite is that the charge separation is activationless, namely in the top region of the Marcus parabola. Here, the effective rate constant remains a function of the electronic coupling matrix. The electronic coupling of C_{60} and porphyrins is a theme of considerable current interest, given the potential applications of the photochemistry peculiar to the resulting systems in optoelectronics.[44−46] The unique topology in the aforementioned $\pi-\pi$ stacks affords electronic couplings in the order of several hundred cm^{-1}. This, in turn, translates into rate constants that exceed 10^{12} s^{-1} and that should compete with the intrinsically fast deactivation seen in several metalloporphyrins.[38]

Now, in this paper, we report the synthesis and physicochemical features of an entire family of redox-active architectures that are built on dendronized C_{60}/porphyrins electron donor−acceptor conjugates.

Results and Discussion

Synthesis and Structural Characterization. The porphyrin core offers the possibility to complex metal atoms by the four central nitrogen centers, which allows for the introduction of additional redox-activity, especially, if transition metals are used. Moreover, the central metal atoms can in principle be used for the binding of axial ligands. Both dyads **H_2-1** and **H_2-2** were used as ligands for Cu, Ni, Co, Fe, and Mn. For the insertion of the metal ions in general a solution of **H_2-1** or **H_2-2** was heated with the corresponding metal chlorides, acetates or acetylacetonates and subsequently purified by column chromatography.[47−49] In this way, the synthesis of the cobalt(II)-dyads **Co(II)-1** and **Co(II)-2** was accomplished by refluxing a solution of the free base dyads in $CHCl_3$ with an excess of $Co(OAc)_2 \cdot 4H_2O$ for a period of 4 h. The nickel(II)-dyads **Ni(II)-1** and **Ni(II)-2** were generated by the thermal treatment of the dyads with Ni(II) acetylacetonate in toluene for 3 h. The corresponding iron(III)- and manganese(III)-dyads **Fe(III)Cl-1**, **Fe(III)Cl-2** and **Mn(III)Cl-1**, **Mn(III)Cl-2**, respectively, were generated using $FeCl_2 \cdot 4H_2O$ and $MnCl_2 \cdot 4H_2O$ as metal

(12) Imahori, H.; Hagiwara, K.; Akiyama, T.; Aoki, M.; Taniguchi, S.; Okada, T.; Shirakawa, M.; Sakata, Y. *Chem. Phys. Lett.* **1996**, *263*, 545.
(13) Guldi, D. M.; Asmus, K.-D. *J. Am. Chem. Soc.* **1997**, *119*, 5744.
(14) Fukuzumi, S.; Ohkubo, K.; Imahori, H.; Guldi, D. M. *Chem.—Eur. J.* **2003**, *9*, 1585.
(15) Guldi, D. M. *Spectrum* **2003**, *16*, 8.
(16) Imahori, H.; Sakata, Y. *Adv. Mater.* **1997**, *9*, 537.
(17) Diederich, F.; Gomez-Lopez, M. *Chem. Soc. Rev.* **1999**, *28*, 263.
(18) Reed, C. A.; Bolskar, R. D. *Chem. Rev.* **2000**, *100*, 1075.
(19) Gust, D.; Moore, T. A.; Moore, A. L. *Acc. Chem. Res.* **2001**, *34*, 40.
(20) Prato, M. *J. Mater. Chem.* **1997**, *7*, 1097.
(21) El-Khouly, M. E.; Ito, O.; Smith, P. M.; D'Souza, F. *J. Photochem. Photobiol., C* **2004**, *5*, 79.
(22) Verhoeven, J. W. *J. Photochem. Photobiol., C* **2006**, *7*, 40.
(23) Boyd, P. D. W.; Reed, C. A. *Acc. Chem. Res.* **2005**, *38*, 235.
(24) Mateo-Alonso, A.; Guldi, D. M.; Paolucci, F.; Prato, M. *Angew. Chem., Int. Ed.* **2007**, *46*, 8120.
(25) D'Souza, F.; Ito, O. *Coord. Chem. Rev.* **2005**, *249*, 1410.
(26) Guldi, D. M.; Rahman, G. M. A.; Sgobba, V.; Ehli, C. *Chem. Soc. Rev.* **2006**, *35*, 471.
(27) Imahori, H. *Bull. Chem. Soc. Jpn.* **2007**, *80*, 621.
(28) Dietel, E.; Hirsch, A.; Eichhorn, E.; Rieker, A.; Hackbarth, S.; Roder, B. *Chem. Commun.* **1998**, 1981.
(29) Schuster, D. I.; Cheng, P.; Jarowski, P. D.; Guldi, D. M.; Luo, C.; Echegoyen, L.; Pyo, S.; Holzwarth, A. R.; Braslavsky, S. E.; Williams, R. M.; Klihm, G. *J. Am. Chem. Soc.* **2004**, *126*, 7257.
(30) Sutton, L. R.; Scheloske, M.; Pirner, K. S.; Hirsch, A.; Guldi, D. M.; Gisselbrecht, J.-P. *J. Am. Chem. Soc.* **2004**, *126*, 10370.

Scheme 1. Insertion of Different Metal Atoms for Synthesis of **M-1** and **M-2**[a]

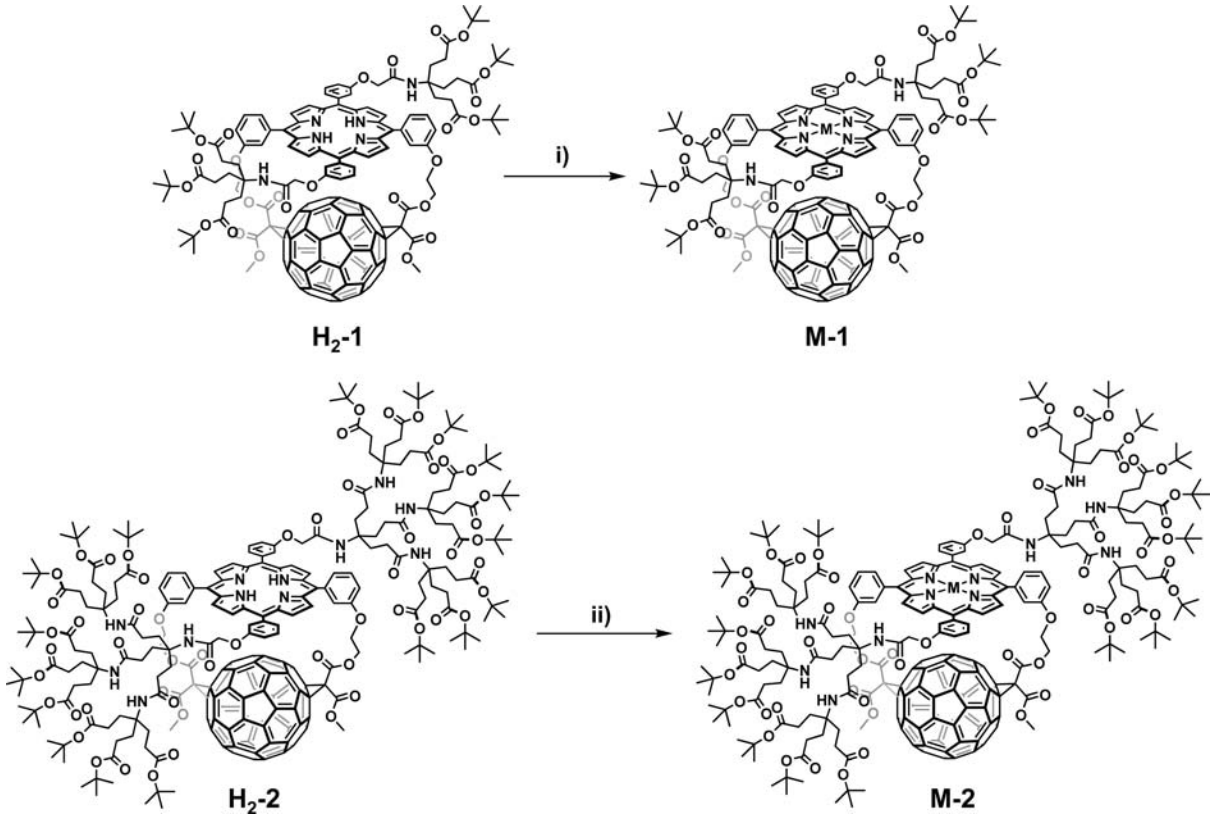

[a] (i) M = Cu: $Cu(OAc)_2$, MeOH, CH_2Cl_2, r.t., 83%; M = Ni: $Ni(acac)_2$, toluene, rf, 75%; M = Co: $Co(OAc)_2 \cdot 2H_2O$, $CHCl_3$, rf, 87%; M = Fe: $FeCl_2 \cdot 4H_2O$, lutidine, EtOH, $CHCl_3$, rf, 98%; M = Mn: $MnCl_2 \cdot 4H_2O$, lutidine, EtOH, $CHCl_3$, rf, 61%; (ii) M = Cu: $Cu(OAc)_2$, MeOH, CH_2Cl_2, r.t., 99%; M = Ni: $Ni(acac)_2$, toluene, rf, 99%; M = Co: $Co(OAc)_2 \cdot 2H_2O$, $CHCl_3$, rf, 77%; M = Fe: $FeCl_2 \cdot 4H_2O$, lutidine, EtOH, $CHCl_3$, rf, 86%; M = Mn: $MnCl_2 \cdot 4H_2O$, lutidine, EtOH, $CHCl_3$, rf, 55%.

salts dissolved in $CHCl_3$/MeOH and lutidine as base. The insertion of copper(II) was carried out by stirring a solution of $Cu(OAc)_2 \cdot 2H_2O$ in methanol with the dyads dissolved in CH_2Cl_2 for 3 h at room temperature to yield **Cu(II)-1** and **Cu(II)-2**. The subsequent purification was accomplished by column chromatography on silica and recrystallization from *n*-pentane. All dyads were obtained in very good yields ranging from 55% to 99%. In the case of iron(III)- and manganese(III)-dyads **Fe(III)Cl-1**, **Fe(III)Cl-2** and **Mn(III)Cl-1**, **Mn(III)Cl-2**, a ligand exchange of the axial chloride by hydroxide was observed after chromatography, which was reverted by washing twice with 2 M HCl, followed by recrystallization from *n*-pentane (Scheme 1).

For a comparison of the redox properties we prepared also the nondendronized analogues of **M-1** and **M-2**. For this purpose, the metal-free dyad **H_2-3**[30] was used as starting material for the synthesis of **Fe(III)Cl-3** and **Mn(III)Cl-3** (Scheme 2).

The synthesis of **M(II)-3** (M = Cu, Ni), however, was carried out by the initial metalation of the free base porphyrin **H_2-4**[28] to give **M(II)-4**. The subsequent cyclopropanation of C_{60} afforded the dyads **M(II)-3** (M = Cu, Ni), which after purification *via* column chromatography on silica were obtained in yields ranging from 37 to 46% (Scheme 3).

As references for photophysical measurements, porphyrin-metal complexes of Cu, Ni, Mn and Fe were required and synthesized according to the aforementioned metal insertion procedures using dyads **M-1** and **M-2**. (Scheme 4).

Electrochemistry. In general, cyclic voltammetry (CV) provides valuable insight into mutual interaction between redox-active molecules; see Table 1. Thus, we performed CV in CH_2Cl_2 containing 0.1 M $(Bu)_4NBF_4$ as supporting electrolyte and ferrocene as an internal standard. A glassy carbon working electrode, a platinum counter electrode, and a silver reference electrode were used. In addition, the potentials were verified by means of differential pulse voltammetry.

Scheme 2. Synthesis of Nondendronized Dyads **M(III)-3** via Precursor **H_2-3**[a]

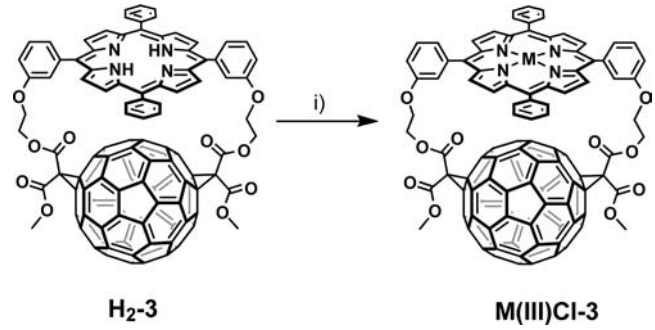

[a] (i) M = Fe: $FeCl_2 \cdot 4H_2O$, lutidine, EtOH, $CHCl_3$, rf, 76%; M = Mn: $MnCl_2 \cdot 4H_2O$, lutidine, EtOH, $CHCl_3$, rf, 63%.

The redox potential for the nondendronized **Zn(II)-3** and **Co(II)-3** are taken from our previous work.[30] The first oxidation processes (E_{ox1}) occur at 0.40 and 0.37 V for **Zn(II)-1** and **Zn(II)-2**, respectively, to yield $[Zn^{II}P]^{\bullet+}$. $[Zn^{II}P]^{2+}$, on the other hand is formed at 0.78 V (E_{ox2}). In the region of reduction processes at −1.09 (E_{red1}), −1.49 (E_{red2}) and −2.04 V (E_{red4}) relate to the reduction of C_{60} to the corresponding radical anion,

Scheme 3. Synthesis of Nondendronized Dyads **M(II)-3** via Precursor **H_2-4**[a]

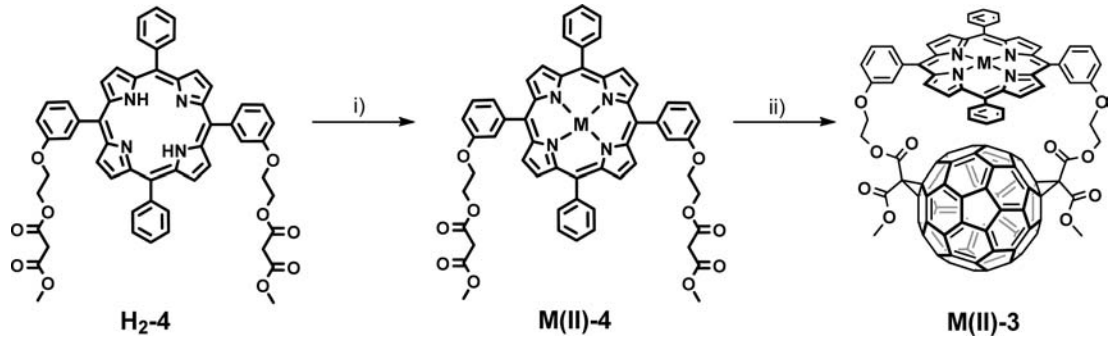

[a] (i) M = Cu: $Cu(OAc)_2$, MeOH, CH_2Cl_2, r.t., 78%; M = Ni: $Ni(acac)_2$, toluene, rf, 82%; (ii) C_{60}, I_2, DBU, toluene, r.t., 46% for M = Cu and 37% for M = Ni.

Scheme 4. Synthesis of metalloporphyrin-precursors **M-5**[a]

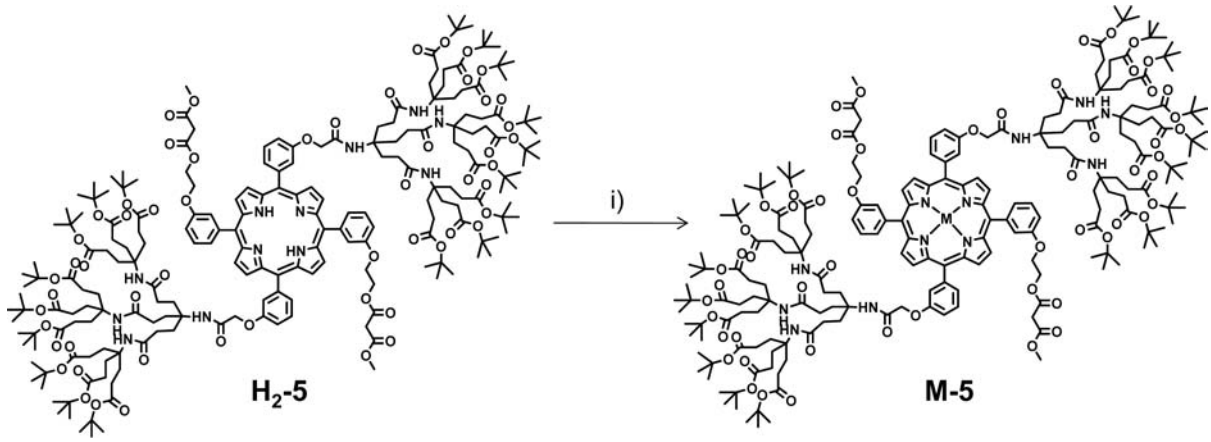

[a] (i) M = Cu: $Cu(OAc)_2$, MeOH, CH_2Cl_2, r.t., 97%; M = Ni: $Ni(acac)_2$, toluene, rf, 95%; M = Fe: $FeCl_2 \cdot 4H_2O$, lutidine, EtOH, $CHCl_3$, rf, 81%; M = Mn: $MnCl_2 \cdot 4H_2O$, lutidine, EtOH, $CHCl_3$, rf, 85%.

dianion and trianion of C_{60}, respectively. The reduction of the porphyrin (E_{red3}) is discernible at −1.86 V for **Zn(II)-1** and at −1.88 V for **Zn(II)-2**.

Co(II)-1 and **Co(II)-2** show three oxidation processes at E_{ox1} = 0.39 V, E_{ox2} = 0.85 V, and E_{ox3} = 1.04 V to lead to $[Co^{III}P]$, $[Co^{III}P]^{2+}$, and $[Co^{III}P]^{3+}$. On the reductive side several redox processes are noted. Whereas the C_{60} reduction involves processes at E_{red1} (−1.01 V for **Co(II)-3**, −0.98 V for **Co(II)-1**, and −1.02 V for **Co(II)-2**), E_{red3} (−1.57 V for **Co(II)-3**, −1.46 V for **Co(II)-1**, and −1.48 V for **Co(II)-2**), and E_{red5} (−1.78 V for **Co(II)-3**, −1.83 V for **Co(II)-1**, and **Co(II)-2**), generating the C_{60} radical anion, C_{60} dianion and C_{60} trianion the $[Co^{II}P]$ reductions are detectable at E_{red2} = −1.33 V and at E_{red4} = −1.70 V.[30]

In the case of **Ni(II)-3**, **Ni(II)-1** and **Ni(II)-2** the first oxidation–at E_{ox1} = 0.55 V for **Ni(II)-3** and E_{ox1} = 0.59 V for **Ni(II)-1** and **Ni(II)-2**–and second oxidation–at E_{ox2} = 0.89 V for **Ni(II)-3** and E_{ox2} = 0.91 V for **Ni(II)-1** and **Ni(II)-2**–generate $[Ni^{II}P]^{\bullet+}$ and $[Ni^{II}P]^{2+}$, respectively. NiP reduction at E_{red3} = −1.90 V for **Ni(II)-3** and approximately at E_{red3} = −1.78 V for **Ni(II)-1** and **Ni(II)-2** generate $[Ni^{II}P]^{\bullet-}$.[50] The C_{60} reduction processes of the fullerene moiety are detectable at E_{red1} (−1.15 V for **Ni(II)-3**, −1.12 V for **Ni(II)-1**, and **Ni(II)-2**), E_{red2} (−1.60 V for **Ni(II)-3**, −1.54 V for **Ni(II)-1**, and −1.55 V for **Ni(II)-2**), and E_{red4} (−1.86 V for **Ni(II)-1** and −1.97 for **Ni(II)-2**).

The first anodic redox processes in **Cu(II)-3**, **Cu(II)-1**, and **Cu(II)-2** (E_{ox1} = 0.49 V for **Cu(II)-3** and about E_{ox1} = 0.53 V for **Cu(II)-1** and **Cu(II)-2**) correspond to the formation of $[Cu^{II}P]^{\bullet+}$. In line with this, the second anodic redox process at E_{ox2} = 0.89 V for **Cu(II)-3**, E_{ox2} = 0.93 V and E_{ox2} = 0.99 V for **Cu(II)-1** and **Cu(II)-2** is assigned to the second oxidation to afford $[Cu^{II}P]^{2+}$. Formation of $[Cu^{II}P]^{\bullet-}$ is only observable for **Cu(II)-1** and **Cu(II)-2** at around E_{red3} = −1.77 V.[51−53] The reductive processes involving C_{60} are detectable at E_{red1} (−1.14 V for **Cu(II)-3**, −1.10 V for **Cu(II)-1** and −1.06 V for **Cu(II)-2**), E_{red2} (−1.61 V for **Cu(II)-3**, −1.53 V for **Cu(II)-1**, and

(31) Chukharev, V.; Tkachenko, N. V.; Efimov, A.; Guldi, D. M.; Hirsch, A.; Scheloske, M.; Lemmetyinen, H. *J. Phys. Chem. B* **2004**, *108*, 16377.
(32) Guldi, D. M.; Hirsch, A.; Scheloske, M.; Dietel, E.; Troisi, A.; Zerbetto, F.; Prato, M. *Chem.—Eur. J.* **2003**, *9*, 4968.
(33) Guldi, D. M.; Luo, C.; Prato, M.; Dietel, E.; Hirsch, A. *Chem. Commun.* **2000**, 373.
(34) Olmstead, M. M.; Costa, D. A.; Maitra, K.; Noll, B. C.; Phillips, S. L.; Van Calcar, P. M.; Balch, A. L. *J. Am. Chem. Soc.* **1999**, *121*, 7090.
(35) Thilgen, C.; Diederich, F. *Chem. Rev.* **2006**, *106*, 5049.
(36) Armaroli, N.; Marconi, G.; Echegoyen, L.; Bourgeois, J.-P.; Diederich, F. *Chem.—Eur. J.* **2000**, *6*, 1629.
(37) Guldi, D. M.; Luo, C.; Da Ros, T.; Prato, M.; Dietel, E.; Hirsch, A. *Chem. Commun.* **2000**, 375.
(38) Guldi, D. M.; Luo, C.; Prato, M.; Troisi, A.; Zerbetto, F.; Scheloske, M.; Dietel, E.; Bauer, W.; Hirsch, A. *J. Am. Chem. Soc.* **2001**, *123*, 9166.
(39) Imahori, H.; Hagiwara, K.; Aoki, M.; Akiyama, T.; Taniguchi, S.; Okada, T.; Shirakawa, M.; Sakata, Y. *J. Am. Chem. Soc.* **1996**, *118*, 11771.

Table 1. Redox Potentials of Metalloporphyrin−Fullerene Dyads versus Fc^+/Fc[a]

		E_{red5} [V]	E_{red4} [V]	E_{red3} [V]	E_{red2} [V]	E_{red1} [V]	E_{ox1} [V]	E_{ox2} [V]	E_{ox3} [V]
Zn	**Zn(II)-3**[30]	−	−2.05	−1.90	−1.51	−1.10	0.34	0.69	−
	Zn(II)-1	−	−2.04	−1.86	−1.45	−1.06	0.40	0.76	−
	Zn(II)-2	−	−2.04	−1.88	−1.49	−1.09	0.37	0.76	−
Co	**Co(II)-3**[30]	−1.78	−	−	−1.57	−1.01	0.40	0.82	0.96
	Co(II)-1	−1.83	−1.70	−1.46	−1.33	−0.98	0.39	0.85	1.04
	Co(II)-2	−1.83	−1.72	−1.48	−1.34	−1.02	0.38	0.85	1.03
Ni	**Ni(II)-3**	−	−1.90	−	−1.60	−1.15	0.55	0.89	−
	Ni(II)-1	−	−1.86	−1.77	−1.54	−1.12	0.59	0.91	−
	Ni(II)-2	−	−1.97	−1.79	−1.55	−1.12	0.59	0.91	−
Cu	**Cu(II)-3**	−	−	−	−1.61	−1.14	0.49	0.89	−
	Cu(II)-1	−	−1.88	−1.79	−1.53	−1.10	0.53	0.93	−
	Cu(II)-2	−	−1.81	−1.76	−1.49	−1.06	0.55	0.99	−
Fe	**Fe(III)Cl-3**	−	−	−1.62	−1.12	−0.81	0.66	−	−
	Fe(III)Cl-1	−1.98	−1.80	−1.51	−1.08	−0.78	0.71	−	−
	Fe(III)Cl-2	−1.91	−1.82	−1.51	−1.10	−0.80	0.71	−	−
Mn	**Mn(III)Cl-3**	−	−	−	−1.20	−0.75	0.72	−	−
	Mn(III)Cl-1	−1.90	−1.63	−1.46	−1.21	−0.76	0.73	−	−
	Mn(III)Cl-2	−1.91	−1.62	−1.45	−1.19	−0.78	0.70	−	−

[a] Electrochemical analysis was carried out in CH_2Cl_2 containing 0.1 M $(Bu)_4NBF_4$ as supporting electrolyte and ferrocene as an internal standard with a glassy carbon working electrode, a platinum counter electrode, and a silver reference electrode.

−1.49 V for **Cu(II)-2**), and E_{red4} (−1.88 V for **Cu(II)-1** and −1.81 for **Cu(II)-2**).

The first oxidation of **Fe(III)Cl-3** is at $E_{ox1} = 0.66$ V, while those of **Fe(III)Cl-1** and **Fe(III)Cl-2** are at $E_{ox1} = 0.71$ V. Although an exact assignment is rather difficult, ligand oxidation to afford $[Fe^{III}(Cl)P]^{\bullet+}$ seems more likely.[54,55] In addition, several reduction processes are detected including the one-electron reduction of Fe^{III} to Fe^{II} around −0.80 V and the one-electron reduction of Fe^{II} to Fe^{I} at approximately $E_{red4} = -1.81$ V.[56] Furthermore, we detected several reductions of C_{60} at E_{red2} (−1.12 V for **Fe(III)Cl-3,** −1.08 V for **Fe(III)Cl-1**, and −1.10 V for **Fe(III)Cl-2**), E_{red3} (−1.62 V for **Fe(III)Cl-3**, −1.51 V for **Fe(III)Cl-1** and **Fe(III)Cl-2**), and E_{red5} (−1.89 V for **Fe(III)Cl-1** and −1.91 V for **Fe(III)Cl-2**).

The only oxidation of **Mn(III)Cl-3**, **Mn(III)Cl-1**, and **Mn(III)Cl-2** happens at $E_{ox1} = 0.72$, 0.73, and 0.70 V, respectively, to form most likely $[Mn^{III}(Cl)P]^{\bullet+}$.[57,58] On the reductive side, reductions of **Mn(III)Cl-3**, **Mn(III)Cl-1**, and **Mn(III)Cl-2** are observed at $E_{red1} = -0.76$ V and $E_{red4} = -1.63$ V. Once again the electrochemistry of C_{60} is apparent in the form of three reduction processes at E_{red2} (−1.20 V for **Mn(III)Cl-3**, −1.21 V for **Mn(III)Cl-1**, and −1.19 V for **Mn(III)Cl-2**), E_{red3} (−1.46 V for **Mn(III)Cl-1** and −1.45 V for **Mn(III)Cl-2**) and E_{red5} (−1.90 V for **Mn(III)Cl-1** and −1.91 V for **Mn(III)Cl-2**).

It should be noted that as the dendrimer generation increases small differences emerge between the formal potentials. Hereby, the strongest shifts are seen between the nondendritic derivatives and the first generation analogue. We find for the cobalt analogues a shift for E_{ox3} of 80 mV for **Co(II)-1** and **Co(II)-2**. In **Fe(III)Cl-1** and **Fe(III)Cl-2** the E_{ox1} potentials shift about 50 mV to a more positive value relative to **Fe(III)Cl-3**. **Cu(II)-1** and **Cu(II)-2** reveal the most significant changes. In fact, E_{ox1} is shifted by 40 and 60 mV for **Cu(II)-1** and **Cu(II)-2**, respectively. Likewise, E_{red1} and E_{red2} are moved about 40 to 80 mV to less negative potentials. The reductive potentials of **Cu(II)-2** are shifted to less negative values and is therefore showing a quite different behavior than the electron donor acceptor conjugate discussed before, where the redox potential of the second generation derivative was hardly shifted. The nickel(II)- and manganese(III)-electron donor acceptor conjugate show no significant change in the formal potential.

It is safe to conclude that the dendritic electron donor acceptor conjugate are more difficult to be oxidized and easier to be reduced when compared with the nondendronized analogues. In our case the influence that the dendritic branches inflict is moderate, because we have chosen a meta-substituted topology. In line with previous work,[59,60] we consider that the slight shifts in the copper and iron electron donor acceptor conjugate relate to the ability of these metal atoms to coordinate the dendron and, in turn, to alter the axial ligation and the redox properties. In the second generation derivatives, two opposing effects might play a role. On one hand, the bulky dendrimer is coordinated to the metal ions, affecting the redox behavior in the mentioned manner. On the other hand, an electron-rich microenvironment is created. This would impose changes on the redox potential in the opposite direction, namely showing a hindered reduction and an easier oxidation.

Electronic Absorption Spectra. When comparing the ground-state absorption features of the different metalloporphyrins in the references and in the corresponding donor−acceptor conjugates notable differences were noted. Most significantly, new absorptions develop in a range, where neither the different metalloporphyrins nor C_{60} is known to absorb, namely beyond 700 nm.[61−63] The fact that the corresponding maxima tend to red-shift with increasing solvent polarity leads us to postulate a redistribution of charge density in the ground state, that is, from the electron-donating metalloporphyrins to the electron accepting C_{60}. Further evidence for this charge transfer hypothesis came from appreciably shifted maxima, especially those of the metalloporphrins. In accordance with the footnote listed in Table 2 we derived the electronic coupling matrix elements (V) for all of the electron donor−acceptor conjugates with values that range from 275 to 520 cm^{-1}.

Fluorescence. Figure 1 shows the fluorescence spectra of **H_2-5**, **H_2-1**, and **H_2-2**, recorded in THF solutions with matching absorption at the excitation wavelength of 392 nm and/or 512 nm. For H_2P (**H_2-5**), we note the well-known emission features, including maxima at 650 and 716 nm, fluorescence quantum yields of 0.11[64,65] and fluorescence lifetimes of 9.8 ns.[66] In **H_2-**

(40) Liddell, P. A.; Sumida, J. P.; Macpherson, A. N.; Noss, L.; Seely, G. R.; Clark, K. N.; Moore, A. L.; Moore, T. A.; Gust, D. *Photochem. Photobiol.* **1994**, *60*, 537.
(41) Guldi, D. M.; Nuber, B.; Bracher, P. J.; Alabi, C. A.; MacMahon, S.; Kukol, J. W.; Wilson, S. R.; Schuster, D. I. *J. Phys. Chem. A* **2003**, *107*, 3215.
(42) Guldi, D. M.; Zilbermann, I.; Gouloumis, A.; Vazquez, P.; Torres, T. *J. Phys. Chem. B* **2004**, *108*, 18485.
(43) *The Porphyrin Handbook*; Kadish, K. M., Smith, K. M., Guilard, R., Eds.; Academic Press: New York, 1999.
(44) Fukuzumi, S.; Guldi, D. M. *Electron Transfer Chem.* **2001**, *2*, 270.
(45) Guldi, D. M. *Chem. Soc. Rev.* **2002**, *31*, 22.
(46) Imahori, H.; Guldi, D. M.; Tamaki, K.; Yoshida, Y.; Luo, C.; Sakata, Y.; Fukuzumi, S. *J. Am. Chem. Soc.* **2001**, *123*, 6617.
(47) Adler, A. D.; Longo, F. R.; Kampas, F.; Kim, J. *J. Inorg. Nucl. Chem.* **1970**, *32*, 2443.
(48) Borovkov, V. V.; Lintuluoto, J. M.; Inoue, Y. *Synlett* **1999**, 61.
(49) Buchler, J. W.; Eikelmann, G.; Puppe, L.; Rohbock, K.; Schneehage, H. H.; Weck, D. *Liebigs Ann. Chem.* **1971**, *745*, 135.
(50) Wolberg, A.; Manassen, J. *Inorg. Chem.* **1970**, *9*, 2365.
(51) Godziela, G. M.; Goff, H. M. *J. Am. Chem. Soc.* **1986**, *108*, 2237.
(52) Kadish, K. M.; Guo, N.; Van Caemelbecke, E.; Paolesse, R.; Monti, D.; Tagliatesta, P. *J. Porphyrins Phthalocyanines* **1998**, *2*, 439.
(53) Wolberg, A.; Manassen, J. *J. Am. Chem. Soc.* **1970**, *92*, 2982.
(54) Bottomley, L. A.; Kadish, K. M. *Inorg. Chem.* **1981**, *20*, 1348.
(55) Phillippi, M. A.; Shimomura, E. T.; Goff, H. M. *Inorg. Chem.* **1981**, *20*, 1322.

Table 2. Electronic Coupling, Reorganization Energies, Charge Separation, and Charge Recombination Dynamics in Different Solvents and the Corresponding Driving Forces

	V^a [cm^{-1}]	λ [eV]	τ_{CS} [ps]	τ_{CR} [ps]	$-\Delta G^0_{CS}$ [eV]	$-\Delta G^0_{CR}{}^c$ [eV]
			H_2-1			
PhMe			150	2200	0.14	1.75
PhCl			130	1500	0.21	1.68
THF	300	0.29	60	860	0.24	1.65
PhCN			40	380	0.27	1.62
DMF			10	115	0.28	1.61
			H_2-2			
PhMe			160	2200	0.14	1.75
PhCl			130	1500	0.21	1.68
THF	300	0.29	60	860	0.24	1.65
PhCN			40	440	0.27	1.62
DMF			10	130	0.28	1.61
			Zn(II)-1			
PhMe			5	370	0.44	1.56
PhCl			4	210	0.51	1.49
THF	520		2	134	0.54	1.46
PhCN			1	40	0.57	1.43
DMF			1	25	0.58	1.42
			Zn(II)-2			
PhMe			5	375	0.44	1.56
PhCl			4	210	0.51	1.49
THF520			2	140	0.54	1.46
PhCN			1	40	0.57	1.43
DMF			1	25	0.58	1.42
			Mn(III)Cl-1			
THF	290	0.61	1	53	0.06	0.35[d]
PhCN			1	46	0.10	0.31[d]
			Mn(III)Cl-2			
PhMe			1	60	0.01	0.40[d]
THF	290	0.61	1	50	0.11	0.30[d]
PhCN			1	45	0.15	0.26[d]
			Fe(III)Cl-1			
PhCN	365[b]	0.55[b]	1	15	0.17	0.23[d]
			Fe(III)Cl-2			
PhCN	365[b]	0.55[b]	1	15	0.17	0.23[d]
			Ni(II)-1			
PhMe			8	115	0.38	0.28[d]
THF	275	0.39	6	80	0.48	0.18[d]
PhCN			3	60	0.52	0.14[d]
			Ni(II)-2			
PhMe			8	115	0.38	0.28[d]
THF	275	0.39	6	80	0.48	0.18[d]
PhCN			3	60	0.52	0.14[d]
			Cu(II)-1			
PhMe			1	>3000	0.40	1.73
THF	405	0.33	1	1600	0.50	1.63
PhCN			1	1200	0.54	1.59
			Cu(II)-2			
PhMe			1	>3000	0.40	1.73
THF	405	0.33	1	1600	0.50	1.63
PhCN			1	1200	0.54	1.59

[a] The electronic coupling (V) was calculated via the following equation out of the ground state absorption in THF. $V = (2.06 \times 10^{-2}\sqrt{(\varepsilon_{max}\tilde{\nu}_{max}\tilde{\nu}_{1/2})})/(R_{C-C})$. R_{C-C} is the center-to-center distance (6.16 Å), ε_{max} is the extinction coefficient of the CT band, ν_{max} is the energy, and $\nu_{1/2}$ is the half width of the CT transition. As noted, the electronic coupling is in all cases distinct. [b] Determined in THF. [c] Charge recombination to the ground state. [d] Charge recombination to the lowest metalloporphyrin tripmultiplet excited state.

1, and **H_2-2** the H_2P fluorescence is quenched 470 times without, however, affecting the overall fluorescence spectrum. The quantum yields for **H_2-1** and **H_2-2** (2.3×10^{-4}) correlates with fluorescence lifetime of 0.25 ps, respectively. ZnP (**Zn(II)-5**), exhibit fluorescence maxima at 600 and 660 nm, a fluorescence

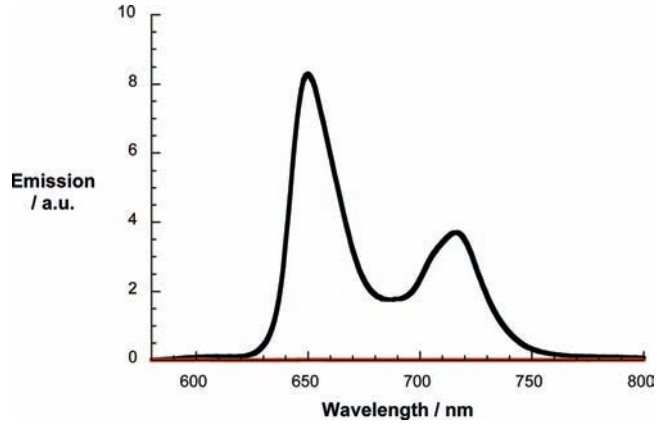

Figure 1. Steady state fluorescence of **H_2-5** (black spectrum), **H_2-1** (red spectrum), and **H_2-2** (red spectrum) excited at 512 nm with matching absorption of the excitation wavelength in deaerated THF ($OD_{512} = 0.11$).

quantum yield of 0.04 and a fluorescence lifetime of 2.4 ns—in excellent agreement with values found in the literature.[32,64,67] The quenching factor, in both **Zn(II)-1** and **Zn(II)-2** (Figure S1), was determined to be 597.

None of the MnP (**Mn(III)Cl-5**), FeP (**Fe(III)Cl-5**), CoP (**Co(II)-5**), NiP (**Ni(II)-5**), and CuP (**Cu(II)-5**) nor the corresponding donor—acceptor conjugates revealed appreciable porphyrin centered fluorescence. A likely rationale involves the paramagnetic nature of the transition metals. To this end, a good overlap between the d orbitals of the metal and the nitrogen lone pairs of the porphyrins triggers ultrafast excited state deactivations.[30,68]

Turning to the 750—850 nm range additional emission features are seen with quantum yields in the order of 10^{-5}—10^{-4}. These are mirror images of the charge transfer absorption and, thus, relate to a charge transfer emission. In **H_2-1** and **H_2-2** solvent dependent maxima evolve at 805 nm, for example, in THF at room temperature; see Figure S2. Interestingly, these features evolve as well in those electron donor—acceptor conjugates that bear transition metals.

The strong charge transfer emissions imply, besides large electronic coupling matrix elements, slow radiative decays and

(56) Kadish, K. M.; D'Souza, F.; Van Caemelbecke, E.; Villard, A.; Lee, J. D.; Tabard, A.; Guilard, R. *Inorg. Chem.* **1993**, *32*, 4179.
(57) Carnieri, N.; Harriman, A. *Inorg. Chim. Acta* **1982**, *62*, 103.
(58) Kelly, S. L.; Kadish, K. M. *Inorg. Chem.* **1982**, *21*, 3631.
(59) Giraudeau, A.; Callot, H. J.; Jordan, J.; Ezhar, I.; Gross, M. *J. Am. Chem. Soc.* **1979**, *101*, 3857.
(60) Kadish, K. M.; Morrison, M. M.; Constant, L. A.; Dickens, L.; Davis, D. G. *J. Am. Chem. Soc.* **1976**, *98*, 8387.
(61) Tkachenko, N. V.; Lemmetyinen, H.; Sonoda, J.; Ohkubo, K.; Sato, T.; Imahori, H.; Fukuzumi, S. *J. Phys. Chem. A* **2003**, *107*, 8834.
(62) Kesti, T. J.; Tkachenko, N. V.; Vehmanen, V.; Yamada, H.; Imahori, H.; Fukuzumi, S.; Lemmetyinen, H. *J. Am. Chem. Soc.* **2002**, *124*, 8067.
(63) Imahori, H.; Tkachenko, N. V.; Vehmanen, V.; Tamaki, K.; Lemmetyinen, H.; Sakata, Y.; Fukuzumi, S. *J. Phys. Chem. A* **2001**, *105*, 1750.
(64) Kuciauskas, D.; Lin, S.; Seely, G. R.; Moore, A. L.; Moore, T. A.; Gust, D.; Drovetskaya, T.; Reed, C. A.; Boyd, P. D. W. *J. Phys. Chem.* **1996**, *100*, 15926.
(65) Lee, W. A.; Graetzel, M.; Kalyanasundaram, K. *Chem. Phys. Lett.* **1984**, *107*, 308.
(66) Tamaki, K.; Imahori, H.; Sakata, Y.; Nishimura, Y.; Yamazaki, I. *Chem. Commun.* **1999**, 625.
(67) Luo, C.; Guldi, D. M.; Imahori, H.; Tamaki, K.; Sakata, Y. *J. Am. Chem. Soc.* **2000**, *122*, 6535.
(68) *The Porphyrin Handbook*; Kadish, K. M., van Camelbecke, E., Royal, G., Eds.; Academic Press: San Diego, 2000; Vol. 8.

small reorganization energies. In fact, the inner ($\lambda_V = (\lambda_{absorption} + \lambda_{emission})/2$) and outer reorganization energies ($\lambda_S = -\lambda_{emission} - \Delta G^0_{CR}$) were derived with the help of the charge transfer absorption ($\lambda_{absorption}$) and emission maxima ($\lambda_{emission}$). These led to total reorganization energies that range from 0.29 eV (**H_2-1**) to 0.61 eV (**Mn(III)-1**)—see Table 2.

Transient Absorption Measurements. To characterize the transients formed upon photoexcitation and upon photodeactivation of either the porphyrins (420 nm) or C_{60} (387 nm), we carried out transient absorption measurements. They were typically performed following femtosecond laser excitation (i.e., 387 or 420 nm) in solvents of different polarity (i.e., toluene, THF, benzonitrile, and DMF).

The visible range of **H_2-5** is in the excited state dominated by intense transitions. Minima as a complement to the ground state absorption evolve at 516, 549, 590, and 648 nm, while maxima are seen at 450, 532, 567, 620, and 674 nm.[67,69] Further out in the red a broad, but nevertheless weak, transient maximizes at around 1050 nm. Within the first few picoseconds (i.e., ~2 ps), higher lying excited states relax to the lowest vibrational state of the first singlet excited state of H_2P. Commencing with this internal conversion, an intersystem crossing starts to set in, which governs the photophysics of **H_2-5** over the course of ~10 ns. The accordingly formed triplet excited state of **H_2-5** reveals a characteristic peak around 780 nm. From here it is only the oxygen sensitive triplet excited state that is generated, for which in the absence of molecular oxygen a lifetime of 380 μs was determined.

When turning to **H_2-1** or **H_2-2** the visible regions are dominated by H_2P centered transitions, while the excited state properties of C_{60} are observed in the near-infrared region. With a delay of 2 ps all of these features (i.e., H_2P and C_{60}) transform into the signatures of the C_{60} radical anion and the H_2P radical cation with characteristic bands at 900 nm and between 550 and 850 nm, respectively. The C_{60} radical anion features of mono- and bis-adducts have been elucidated in great details and appear for the *trans-2* adduct with a maximum at 900 nm.[70] The H_2P radical cation, on the other hand, needed independent characterization by means of pulse radiolysis, where the corresponding species were obtained upon one electron oxidation in either oxygenated or deoxygenated solutions of dichloromethane. As a matter of fact, the radiolytic signature (i.e., transient maximum between 550 and 850 nm) closely resembles that seen in the current photolytic experiments run with **H_2-1** or **H_2-2**. With this spectroscopic confirmation in hands we analyzed the time absorption profiles in terms of charge separation and charge recombination kinetics. The lifetimes (see Figure 2) are in THF 60 (i.e., charge separation) and 860 ps (i.e., charge recombination). By increasing (i.e., benzonitrile) or decreasing (i.e., toluene) the solvent polarity the driving forces for charge separation and charge recombination change. This affects the lifetimes in benzonitrile with values of 40 and 380 ps, while in toluene the lifetimes are 150 and 2100 ps.

When turning to ZnP (**Zn(II)-5**), the following features form instantaneously. A minimum, due to Q-band bleaching, is generated at 550 nm followed by maxima in the visible region at 500 nm, as well as between 570 and 740 nm and in the near-infrared region between 900 and 1000 nm. Within 2.4 ns, these singlet excited state features transform into those of the

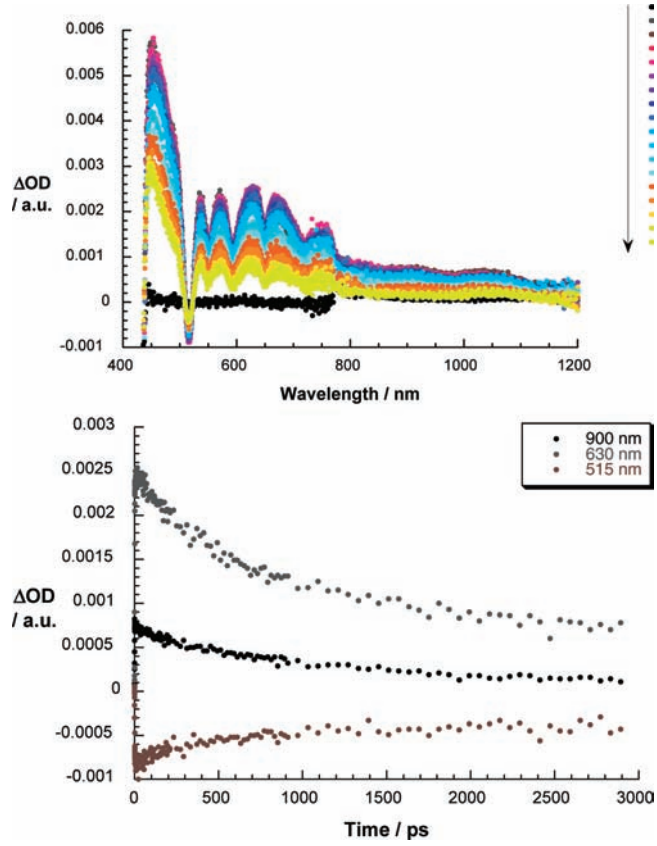

Figure 2. (Top) Differential absorption spectra (visible and near-infrared) obtained upon femtosecond flash photolysis (420 nm, 100 nJ) of **H_2-2** (~10^{-6} M) in argon saturated THF with several time delays between 0 and 3000 ps at room temperature; see legend for time evolution. (Bottom) Time absorption profiles at 515, 630, and 900 nm of the spectra shown above, monitoring the charge separation and charge recombination.

0.51 eV lower-lying triplet excited state.[32,67,71] An intersystem crossing with an efficiency of 0.88 powers this conversion. The correspondingly formed triplet, with a maximum at 860 nm, is oxygen sensitive and typically lasts for tens of microseconds (i.e., 44 μs).

At early times the transients formed upon exciting **Zn(II)-1** and **Zn(II)-2** are practically identical to those seen in the case of ZnP (**Zn(II)-5**); see Figure 3. After a time delay of 1 ps a new broad transition starts to develop. The latter include maxima in the visible range between 580 and 800 nm and in the near-infrared range at 900 nm. A spectral comparison with previous pulse radiolytic investigations helps to assign the set of visible maxima to the ZnP radical cation,[32,67] while the 900 nm band, as already seen, is ascribed to the C_{60} radical anion.[70] In THF, charge separation and charge recombination take place with 2 and 140 ps, respectively. However, the lack of notable ZnP triplet excited state formation suggests that the charge separated states recombine directly to the ground state. Using toluene resulted in longer lifetimes (i.e., 375 ps), while in benzonitrile shorter lifetimes (i.e., 80 ps) were determined for the charge separated state. Charge separation is similarly affected with 5 ps in toluene and 1 ps in benzonitrile.

Next, we turned to MnP (**Mn(III)Cl-5**) and **Mn(III)Cl-1**/**Mn(III)Cl-2**. Important is the nature of the ground state, $^5S_0$.[72]

(69) Rodriguez, J.; Kirmaier, C.; Holten, D. *J. Am. Chem. Soc.* **1989**, *111*, 6500.
(70) Guldi, D. M.; Asmus, K.-D. *J. Phys. Chem. A* **1997**, *101*, 1472.
(71) Imahori, H.; Tamaki, K.; Guldi, D. M.; Luo, C.; Fujitsuka, M.; Ito, O.; Sakata, Y.; Fukuzumi, S. *J. Am. Chem. Soc.* **2001**, *123*, 2607.
(72) Yan, X.; Kirmaier, C.; Holten, D. *Inorg. Chem.* **1986**, *25*, 4774.

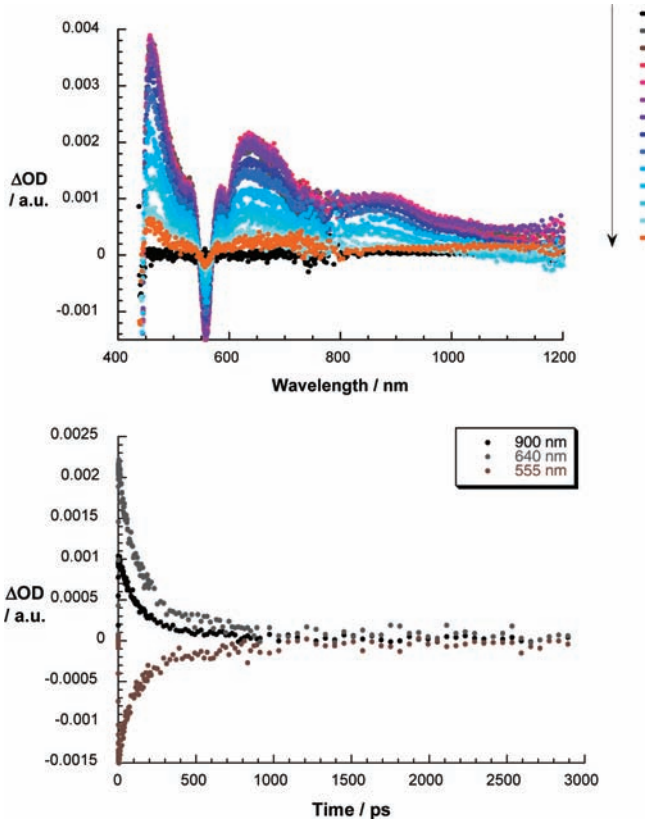

Figure 3. (Top) Differential absorption spectra (visible and near-infrared) obtained upon femtosecond flash photolysis (420 nm, 100 nJ) of **Zn(II)-2** ($\sim 10^{-6}$ M) in argon saturated THF with several time delays between 0 and 500 ps at room temperature; see legend for time evolution. (Bottom) Time absorption profiles at 555, 640, and 900 nm of the spectra shown above, monitoring the charge separation and charge recombination.

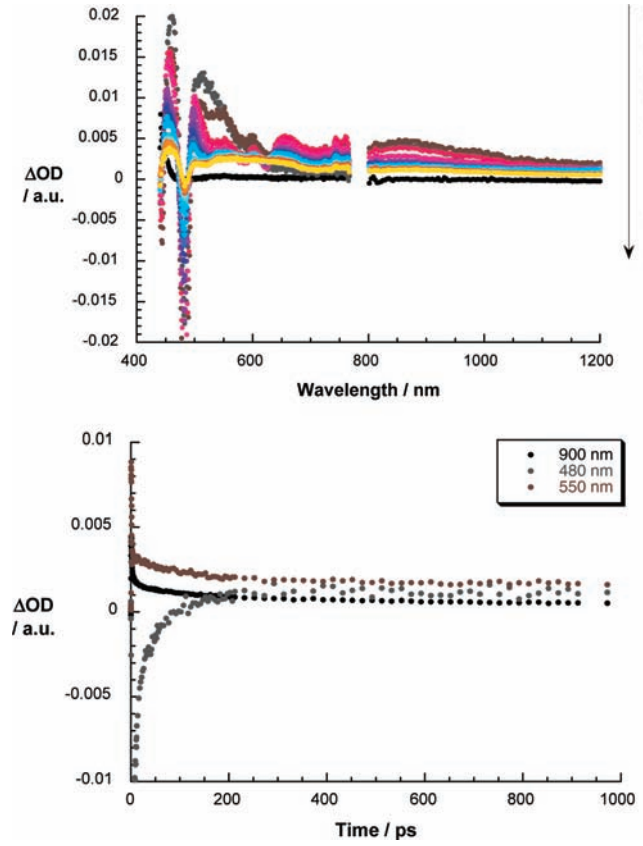

Figure 4. (Top) Differential absorption spectra (visible and near-infrared) obtained upon femtosecond flash photolysis (387 nm, 150 nJ) of **Mn-(III)Cl-2** ($\sim 10^{-6}$ M) in argon saturated PhCN with several time delays between 0 and 3 ns at room temperature; see legend for time evolution. (Bottom) time absorption profiles at 480, 550, and 900 nm of the spectra shown above, monitoring the charge separation and charge recombination.

Directly following the laser pulse (Figure S3) MnP reveals minima at 570 and 620 nm as a kind of negative imprint of the ground state absorption. In addition, maxima are seen from 430 to 550 nm and beyond 645 nm.[72] Implicit is the rapid formation of a tripquintet ($^5T_1$) excited state. The initially formed $^5S_1$ state, on the other hand, was not observable, since the $^5S_1$ to $^5T_1$ transfer happens essentially within the detection limit of our instrumental resolution as a consequence of efficient coupling to the tripquinted state.[72] Within the time window of the next 30 ps two deactivation processes compete: the spin allowed recombination to the ground state ($^5S_0$) and spin conversion to the tripheptet excited state ($^7T_1$).[73] The recombination to the ground state is heavily favored by very good overlaps between the porphyrin (π, π*) and the manganese (d, d*) orbitals,as well as by interactions with several charge transfer states.[72,73] $^7T_1$, formed in minor amounts, decays within 70 ps to the ground state.

Figure 4 documents that the features developing for **Mn-(III)Cl-1** and **Mn(III)Cl-2** differ from those of **Mn(III)Cl-5**. Particularly important is the red region with a broad transition that extends from 650 nm all the way to 1200 nm. A closer look discloses the signature of the C_{60} radical anion, again, at 880 nm,[70] together with another maximum at 695 nm, which is tentatively assigned to the MnP radical cation (Figure S4). The small blue-shift is likely to result from interactions with the manganese. In the blue region, on the other hand, the imprint of the ground state absorption is noticeable. Overall, a good spectral resemblance with the features seen during the pulse radiolysis study, that is, the one-electron oxidation and one-electron reduction of MnP and C_{60}, respectively, confirms the charge transfer mechanism. Charge recombination populates the triplet excited state and takes place within 50 ps in THF. On the other hand, varying the solvent polarity from toluene to benzonitrile led to a trend that tracks those already discussed for **H_2-1**, **H_2-2**, **Zn(II)-1**, and **Zn(II)-2**. In brief, the lifetimes decrease from 60 (i.e., toluene) to 45 ps (i.e., benzonitrile).

The transient absorption features of FeP (**Fe(III)Cl-5**) (Figure S5) include in the visible region maxima at >490, 540, and 632 nm and ground state bleaching at 570 nm.[74] In the near-infrared region of the spectrum a maximum around 900 nm is discernible directly after the laser excitation. Please note the resemblance of this feature with the triplet markers in general. The instantaneously formed $^6S_1$ decays, like in **Mn(III)Cl-5**, rapidly to the triphexet ($^6T_1$) state, again facilitated by an orbital and spin allowed process.[74] Following the formation of $^6T_1$, recombination to the ground state and internal conversion to other tripmultiplets compete in the next 6 ps. Once more, the good overlap between porphyrin (π, π*) and metal (d, d*) orbitals together with possible charge transfer states lead to an intrinsically fast deactivation of the triphexet. Afterward, the tripoctet ($^8T_1$) excited state follows a relaxation pathway to generate the ground state within 25 ps.[74]

(73) Harriman, A. *J. Chem. Soc., Faraday Trans. 1* **1981**, *77*, 369.

(74) Cornelius, P. A.; Steele, A. W.; Chernoff, D. A.; Hochstrasser, R. M. *Chem. Phys. Lett.* **1981**, *82*, 9.

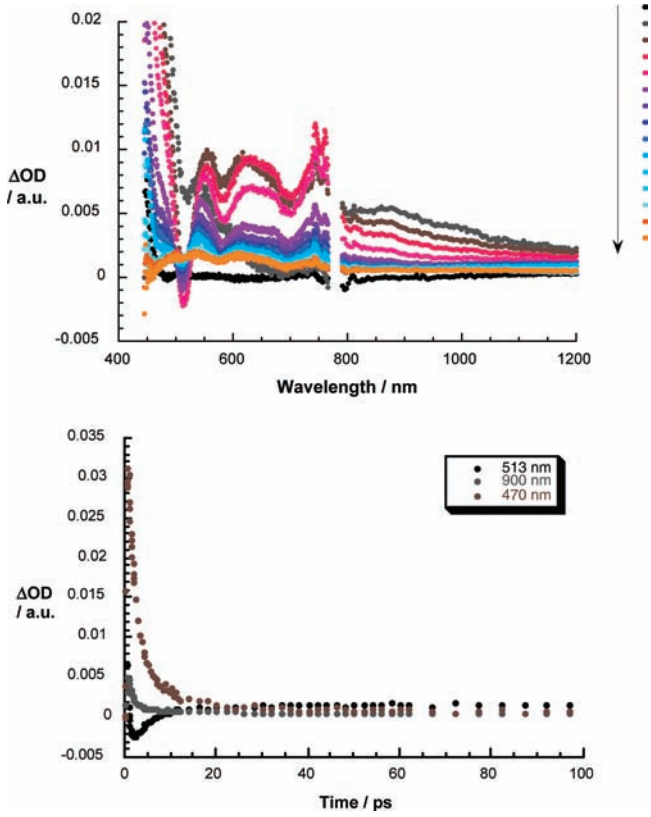

Figure 5. (Top) differential absorption spectra (visible and near-infrared) obtained upon femtosecond flash photolysis (387 nm, 150 nJ) of **Fe(III)Cl-2** ($\sim 10^{-6}$ M) in argon saturated benzonitrile with several time delays between 0 and 50 ps at room temperature; see legend for time evolution. (Bottom) Time absorption profiles at 470, 513, and 900 nm of the spectra shown above, monitoring the charge separation and charge recombination.

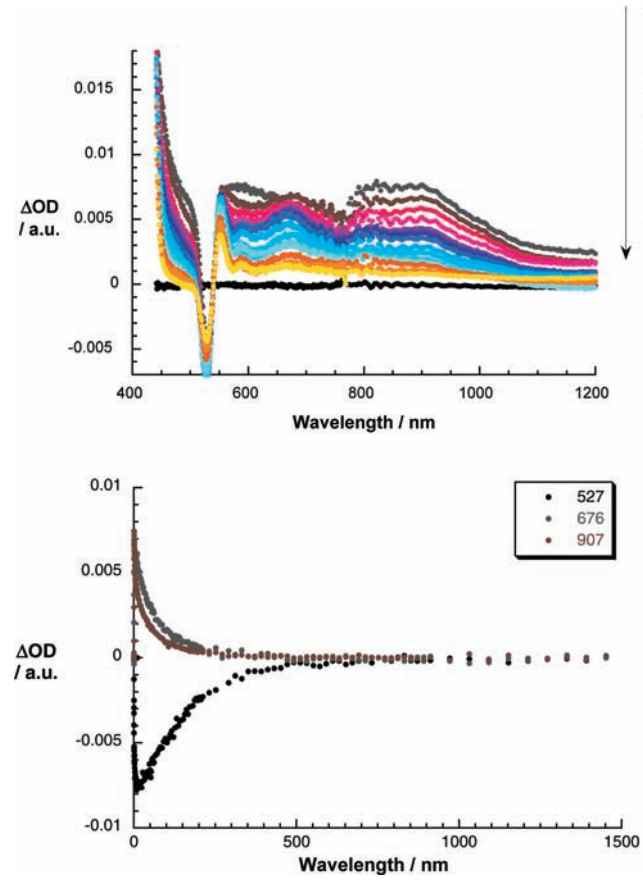

Figure 6. (Top) Differential absorption spectra (visible and near-infrared) obtained upon femtosecond flash photolysis (420 nm, 100 nJ) of **Ni(II)-2** ($\sim 10^{-6}$ M) in argon saturated THF with several time delays between 0 and 500 ps at room temperature; see legend for time evolution. (Bottom) time absorption profiles at 527, 676, and 907 nm of the spectra shown above, monitoring the charge separation and charge recombination.

In **Fe(III)Cl-1** and **Fe(III)Cl-2** (Figure 5), we note that essentially commencing with the excitation the aforementioned excited state features transform into a new transient. The spectral features of this newly formed transient, namely a broadband red-shifted with regard to the long wavelength absorption (i.e., 600−850 nm), are similar to the radiolytically formed FeP radical cation, which is shown in Figure S6. This suggests a rapid intramolecular charge transfer to oxidize FeP. Detecting around 880 nm the fingerprint of the C_{60} radical anion[70] completes also in this case the characterization of the charge separated state. Again, the small blue-shift, relative to **Zn(II)-2**, is likely to result from interactions with the metal center. The charge separated states recombines within 15 ps to afford the triplet excited state rather than the ground state.

The transient absorption for NiP (**Ni(II)-5**) at around 1 ps shows excited state bleaching at 520 nm and excited state absorption in the 430−500 nm region and above 540 nm (Figure S7). Subsequently, the transient feature narrow and blue shift within the next 20 ps and finally deactivate to the ground state within 200 ps. The individually resolved steps are formation of a singlet excited state, very fast intersystem crossing to form a hot T_1 state, a vibrational relaxation to the relaxed T_1 excited state and deactivation to the ground state.[69,75]

In Figure 6 the same singlet excited state features, as they were seen for **Ni(II)-5**, develop directly after the laser excitation of **Ni(II)-1** and **Ni(II)-2**. Now, the very fast intersystem crossing (20 ps) competes with the charge separation. In fact, after about 2 ps features of the NiP radical cation and of the C_{60} radical anion[70] were seen at 650 and 900 nm, respectively. Confirmation for this assignment came from pulse radiolytic investigations (Figure S8) which resulted in a differential absorption maximum that ranges from 540 to 730 nm. Kinetically, 6 and 80 ps were determined for the charge separation and charge recombination in THF. In line with the Marcus inverted behavior, charge recombination takes values of 115 ps in toluene (a stabilization) and 60 ps in benzonitrile (a destabilization). Charge separation, on the other hand, slows down in toluene and accelerates in benzonitrile.

CuP (**Cu(II)-5**) is different: Upon photoexcitation of the ground ($^2S_0$) state, triplet excited state features grow in instantaneously giving rise to excited state bleaching at 540 nm and excited state absorption from 430 to 530 nm followed by a maximum at 825 nm.[41,69] This is documented in Figure S9. In particular, the latter one is a known characteristic for triplets of many porphyrins (i.e., free base porphyrins and metalloporphyrins). In fact it is a tripdoublet ($^2T_2$) state that is formed rapidly, in very high quantum yields of about 88% ± 2%[76], from a singdoublet precursor, since the underlying conversion is orbital and spin allowed. Now $^2T_2$ deactivates via a series of competing channels: these include internal conversion yielding $^2T_1$, intersystem crossing to the tripquartet ($^4T_2$ or $^4T_1$) state or

(75) Zhang, X.; Wasinger, E. C.; Muresan, A. Z.; Attenkofer, K.; Jennings, G.; Lindsey, J. S.; Chen, L. X. *J. Phys. Chem. A* **2007**, *111*, 11736.
(76) Pineiro, M.; Carvalho, A. L.; Pereira, M. M.; Gonsalves, A. M.; d, A. R.; Arnaut, L. G.; Formosinho, S. J. *Chem.—Eur. J.* **1998**, *4*, 2299.

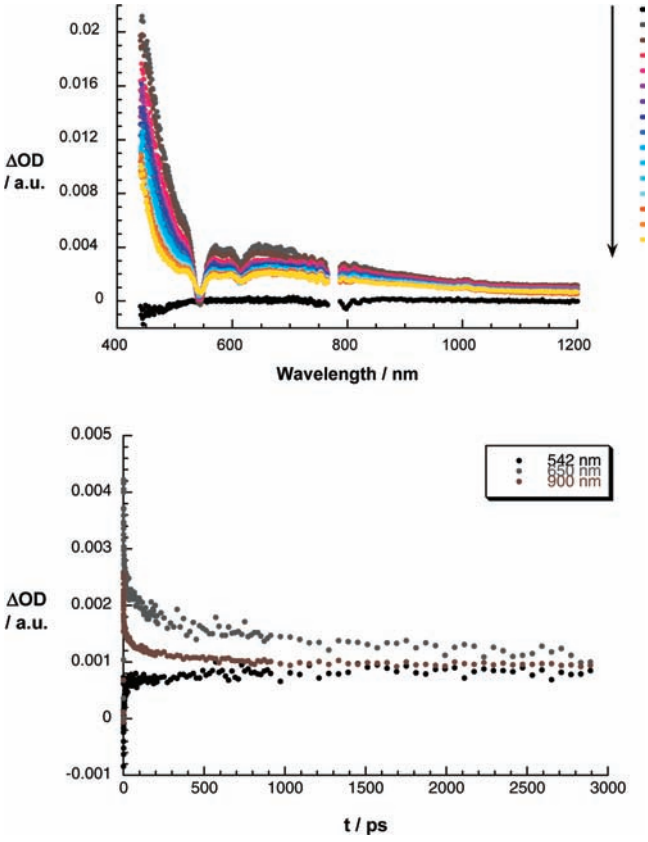

Figure 7. (Top) Differential absorption spectra (visible and near-infrared) obtained upon femtosecond flash photolysis (420 nm, 100 nJ) of **Cu(II)-2** ($\sim 10^{-6}$ M) in argon saturated THF with several time delays between 0 and 500 ps at room temperature; see legend for time evolution. (Bottom) Time absorption profiles at 542, 650, and 900 nm of the spectra shown above, monitoring the charge separation and charge recombination.

deactivation to $^2S_0$, which is the ground state.[41,69] Notable, these deactivation pathways are solvent dependent, 545 ps in benzonitrile, 250 ps in THF and >3 ns in non-coordinating solvents. Coordinating solvents affect the orbital energies of, for example, the charge transfer state and tend to quench the triplet excited states.[41]

In stark contrast to the CuP reference, **Cu(II)-1** and **Cu(II)-2** are both subject to very fast charge separation processes in THF and benzonitrile (Figure 7). The time window during which the charge separation occurs is about 1 ps. While in THF a weak transient for a competing triplet excited state was observable in addition to the charge separated state, in benzonitrile just the signature of the charge separated state with maxima at 650 and 900 nm occurred. Pulse radiolytic oxidation, conducted with CuP (Figure S10), further confirmed these characteristics, that is, a transient maximum between 550 and 800 nm. Lifetimes of the charge separated state were 1.6 and 1.2 ns in THF and benzonitrile, respectively. In THF, the minor formed triplet excited states deactivate within 160 ps. In toluene, on the other hand, the lack of evidence for any charge transfer reaction suggests that this deactivation channel is shut down for **Cu(II)-1** and **Cu(II)-2**.

Energetics. The H_2P singlet excited state is located in **H_2-5**, **H_2-1**, and **H_2-2** at 1.89 eV.[67] Once formed, several different deactivation channels are feasible. One of them is charge separation, at least for **H_2-1** and **H_2-2**, to yield the corresponding charge-separated state (1.53 eV). The latter may, in fact, also evolve from the C_{60} singlet excited state (1.79 eV).[77] It is also notable that the two singlet excited states may interact via transduction of singlet excited state energy. The correspondingly formed charge separated state recombines competitively to the lower lying H_2P triplet excited state (1.4 eV)[67] or to the ground state. Evidence for a possible C_{60} triplet excited state (1.5 eV)[70,78] formation was not observed during our measurements.

In **Zn(II)-1** and **Zn(II)-2** charge separation that commences from the instantaneously formed ZnP singlet excited state (2.04 eV)[32,67] is strongly exothermic (0.76 eV). Such a driving force places the underlying charge transfer into the top region of the Marcus parabola, where it would be activationless. Even a charge separation that would commence with the C_{60} singlet excited state (1.79 eV) is still fairly exothermic with 0.51 eV. The charge recombination takes an interesting twist. In polar media the only exothermic pathway is the direct recovery of the singlet ground state. On the other hand, in nonpolar media, formation of the ZnP triplet excited state is thermodynamically within reach.

In **Mn(III)Cl-1** and **Mn(III)Cl-2** the deactivation upon photoexcitation follows closely that of **Mn(III)Cl-5**. The initially formed singquinted excited state ^{1}*S_5 (2.01 eV)[79] decays within 0.1−0.5 ps, mainly via internal conversion to the ground state.[80] The other competing processes are: The deactivation via the charge separated state at 1.9 eV in **Mn(III)Cl-1** and **Mn(III)Cl-2**, or the spin allowed intersystem crossing to the tripquinted excited state (^{1}*T_5)(1.80 eV), or the spin forbidden intersystem crossing to the triphepted excited state (^{1}*T_7)(1.60 eV).[73,79,81,82] Considering the weak driving force for charge separation of 0.1 eV in THF, charge separation occurs only in low yields. Notably, even the use of more polar media fails in improving the situation, 0.15 eV in benzonitrile. The dominant deactivation is the internal conversion like in **Mn(III)Cl-5**.

The energetics of **Fe(III)Cl-1** and **Fe(III)Cl-2** bear close resemblance to what has been seen for **Mn(III)Cl-1** and **Mn(III)Cl-2**. The initially formed singhexet excited state (^{1}*S_6), located at 1.94 eV[79], deactivates in toluene to the at 1.78 eV[73] located triphexet excited state (^{1}*T_6) in less than 1 ps. Overall, such an acceleration is based on strong orbital interactions (d−d*, d−d, CT, $\pi-\pi$*) and overlaps. The triphexet excited state (^{1}*T_6) recovers either directly or via the 0.24 eV[73,79] lower lying tripocted excited state to the ground state. In benzonitrile, the charge separated state is located at 1.77 eV and, in turn, 0.01 eV below the triphexet excited state. In fact, charge separation competes in **Fe(III)Cl-1** and **Fe(III)Cl-2** with the formation of the triphexet excited state. Charge recombination, on the other hand, to the tripocted excited state is located with 0.23 eV in the Marcus normal region.

In **Ni(II)-5** the initially formed singlet excited state ^{2}*S (3.11 eV)[83] decays ultrafast[79,83,84] to form a hot triplet excited state ^{3}(d, d). In the next step an intermolecular redistribution of energy

(77) Guldi, D. M.; Hauke, F.; Hirsch, A. *Res. Chem. Intermed.* **2002**, *28*, 817.
(78) Foote, C. S. *Top. Curr. Chem.* **1994**, *169*, 347.
(80) Irvine, M. P.; Harrison, R. J.; Strahand, M. A.; Beddard, G. S. *Ber. Bunsen-Ges. Phys. Chem.* **1985**, *89*, 226.
(81) Becker, R. S.; Allison, J. B. *J. Phys. Chem.* **1963**, *67*, 2662.
(82) Harriman, A.; Porter, G. *J. Chem. Soc., Faraday Trans. 2* **1979**, *75*, 1543.
(79) Brookfield, R. L.; Ellul, H.; Harriman, A. *J. Chem. Soc., Faraday Trans. 2* **1985**, *81*, 1837.
(83) Patchkovskii, S.; Kozlowski, P. M.; Zgierski, M. Z. *J. Chem. Phys.* **2004**, *121*, 1317.
(84) Chen, L. X.; Zhang, X.; Wasinger, E. C.; Attenkofer, K.; Jennings, G.; Muresan, A. Z.; Lindsey, J. S. *J. Am. Chem. Soc.* **2007**, *129*, 9616.

through vibrational cooling results in a relaxed triplet excited state, which is followed by ground-state recovery.[75] In **Ni(II)-1** and **Ni(II)-2**, the first step is assigned to a very fast charge separation, which benefits from a good orbital overlap. The charge separated state, located at 1.72 eV in THF, recombines afterward to the relaxed triplet excited state. The driving force for the charge recombination to the triplet excited state, which should be located between 1.5 and 1.6 eV (0.7 eV below the singlet excited state[83]), is about 0.18 eV.

Before examining the deactivation pathways that occur in **Cu(II)-1** and **Cu(II)-2**, the processes taking place in **Cu(II)-5** have to be considered briefly. The instantaneously formed singdoublet excited state, located around 2.13 eV,[73,79,85] decays rapidly in **Cu(II)-5** in less than 350 fs[69,86,87] to the tripdoublet excited state which is located between 1.70 and 1.64 eV (1.70,[76] 1.66,[73] 1.64 eV for tripdouble−tripquartet equilibrium).[41] Next, the triplet and CT states equilibrate via a spin-forbidden intersystem crossing to the 0.07 eV lower lying tripquartet excited state (1.59 eV).[73,79] The tripquartet excited state deactivates afterward to the singdoublet ground state. In **Cu(II)-1** and **Cu(II)-2**, the charge separated state is located marginally below that of the tripdoublet excited state at 1.63 eV. Nevertheless, strong interactions as they prevail between the porphyrin ($\pi-\pi^*$) orbitals and the copper (d−d*) orbitals accelerate the charge separation. Taking the driving force for the charge recombination to the tripdoublet excited state into consideration, we estimate values of around 0.04 eV. In contrast, recovery of the ground state is strongly exergonic and, thus, placed deeply in the Marcus inverted region. Important is that shifting the energy of the charge separated state–by, for instance, varying the solvent polarity–above the tripdoublet state (toluene) or below the tripquarted state (PhCN), charge separation remains to be fast. In all of the cases the charge separated state recombines to the ground state as it is reflected by the experimental data. In other words, the driving force for the charge separation is located in the top region of the Marcus parabola, while the driving force for the charge recombination is deeply in the Marcus inverted region.

Conclusion

In summary, we report here on the synthesis and charge transfer features of an entire new family of redox-active electron donor−acceptor architectures. In particular, we have developed dendronized metal porphyrins attached to C_{60} via a *trans-2* addition pattern by choosing Newkome-type dendrons of first and second generations bound in the meta positions of the two free phenyl rings. Most importantly, we have succeeded for the first time in probing metalloporphyrins bearing manganese(III), iron(III), nickel(II), and copper(II). A key feature is the close distance, $\pi-\pi$ stacking, that separates the excited state electron donor from the electron acceptor. In fact, this $\pi-\pi$ stacking motif emerged as a powerful means to overcome the intrinsically fast deactivation of the excited states in these metalloporphyrins. The lifetimes of the rapidly and efficiently generated radical ion pair states were found to depend on (i) the solvent polarity and (ii) the metal species. To this end, they are as short as 15 ps when a tripmultiplet excited state is formed and reach to values that are beyond 3000 ps when the ground state is regenerated. Most important is, however, that a correlation between the charge transfer rate (i.e., charge separation and charge recombination) and the free energy change for the underlying reaction reveals a parabolic dependence, as illustrated in Figure 8, with parameters of the reorganization energy (0.84 eV) and electronic coupling (70 cm^{-1}) closely resembling those seen for the zinc(II)/free-base analogues studied in recent work and those derived from the charge transfer absorptions/charge transfer emissions. This particular finding is of a great value, since it assists in establishing the Marcus relationship not only by varying the solvent polarity but also by changing the metal species. In other words it overcomes the drawbacks as they stem from largely different outer reorganization energies (i.e., solvent contributions) when screening toluene, orthodichlorobenzene, benzonitrile, etc., while emphasizing the role of the internal reorganization energies (i.e., structural contributions) in C_{60}-based electron donor−acceptor conjugates/hybrids.

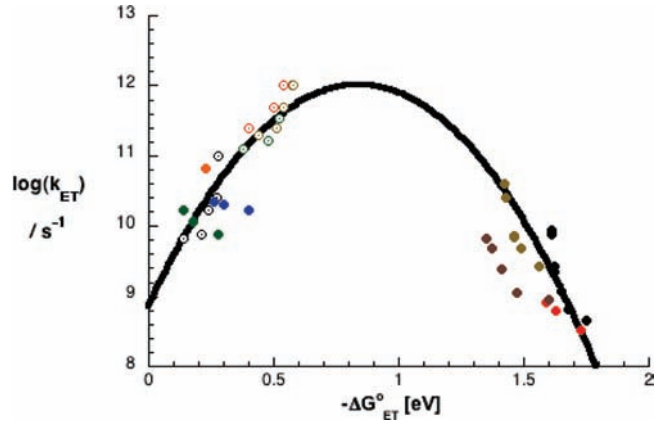

Figure 8. Driving force ($-\Delta G^0_{ET}$) dependence of the rate constant for charge separation (open circles) and charge recombination (full circles) in **Mn(III)Cl-1**, **Mn(III)Cl-2** (blue symbols), **Fe(III)Cl-1**, **Fe(III)Cl-2** (orange symbols), **Co(II)-3** (grey symbols),[30] **Ni(II)-1**, **Ni(II)-2** (green symbols), **Cu(II)-1**, **Cu(II)-2** (red symbols), **Zn(II)-1**, **Zn(II)-2** (brown symbols), **H_2-1**, and **H_2-2** (black symbols).

Acknowledgment. This work was supported by the Deutsche Forschungsgemeinschaft through SFB583.

Supporting Information Available: Steady-state fluorescence spectra of **Zn(II)-5**, **Zn(II)-1**, and **Zn(II)-2**; charge transfer absorption and emission spectra of **H_2-1** and **Cu(II)-1**; differential absorption spectra, time absorption profiles, pulse radiolytic oxidation of the metalloporphyrin references **Mn(III)Cl-5**, **Fe(III)Cl-5**, **Ni(II)-5**, and **Cu(II)-5**; and experimental details. This material is available free of charge via the Internet at http://pubs.acs.org.

JA9029686

(85) Seybold, P. G.; Gouterman, M. *J. Mol. Spectrosc.* **1969**, *31*, 1.
(86) LeCours, S. M.; Philips, C. M.; de Paula, J. C.; Therien, M. J. *J. Am. Chem. Soc.* **1997**, *119*, 12578.
(87) Yan, X.; Holten, D. *J. Phys. Chem.* **1988**, *92*, 5982.